Earth and Planetary Science Letters 501 (2018) 165–179

Contents lists available at ScienceDirect

Earth and Planetary Science Letters

www.elsevier.com/locate/epsl

Tracking variable sedimentation rates and astronomical forcing in Phanerozoic paleoclimate proxy series with evolutionary correlation coefficients and hypothesis testing

Mingsong Li [a,*], Lee R. Kump [a], Linda A. Hinnov [b], Michael E. Mann [a]

[a] Department of Geosciences, The Pennsylvania State University, University Park, PA 16802, USA
[b] Department of Atmospheric, Oceanic, and Earth Sciences, George Mason University, Fairfax, VA 22030, USA

ARTICLE INFO

Article history:
Received 18 April 2018
Received in revised form 19 August 2018
Accepted 23 August 2018
Available online xxxx
Editor: D. Vance

Keywords:
sedimentation rate
astronomical forcing
Paleocene–Eocene Thermal Maximum
Late Triassic
Devonian

ABSTRACT

This paper addresses two fundamental issues in cyclostratigraphy and paleoclimatology: identification of astronomical forcing in sequences of stratigraphic cycles, and accurate evaluation of variable sedimentation rates. The technique presented here considers these issues part of an inverse problem and estimates the product-moment correlation coefficient between the power spectra of astronomical solutions and paleoclimate proxy series across a range of test sedimentation rates. The number of contributing astronomical parameters in the estimate is also considered. Our estimation procedure tests the hypothesis that astronomical forcing had a significant impact on proxy records. The null hypothesis of no astronomical forcing is evaluated using a Monte Carlo simulation approach. The test is applied using a sliding stratigraphic window to track variable sedimentation rates along the paleoclimate proxy series, in a procedure termed "eCOCO" (evolutionary correlation coefficient) analysis. Representative models with constant and variable sedimentation rates, and pure noise and mixed signal and noise series are evaluated to demonstrate the robustness of the approach. The method is then applied to Cenozoic, Mesozoic and Paleozoic paleoclimate series. The Cenozoic case study focuses on a high-resolution Paleocene–Eocene iron concentration series from ODP Site 1262 (Leg 208) covering the Paleocene–Eocene Thermal Maximum and Eocene Thermal Maximum 2 events. The eCOCO time-calibrated iron series confirms previous findings of a role for long-term astronomical forcing of these Eocene events. The Mesozoic case study applies eCOCO to the classic Late Triassic Newark depth rank series of eastern North America. The estimated high-resolution sedimentation rate map in this case demonstrates a causal link between variations in depositional environment and sedimentation rate. Finally, the Paleozoic case study supports the cyclostratigraphic interpretation of a Devonian magnetic susceptibility series at La Thure, Belgium and provides new insights into changes of the depositional setting at this location. Taken together, eCOCO is a powerful tool for simultaneously evaluating sedimentation rates and astronomical forcing for paleoclimate series throughout the Phanerozoic.

1. Introduction

Construction of the geological time scale includes multiple sources and methods, radioisotopic dating, biostratigraphy, magnetostratigraphy, chemostratigraphy, cyclostratigraphy, and mathematical modeling. Among these techniques, the cyclostratigraphic analysis of Milankovitch cycles is the only method that can provide continuous, high-resolution age models (Gradstein et al., 2012). Numerous sedimentary records are evidently impacted by Milankovitch forcing at timescales of tens to hundreds of thousands of years (Hinnov, 2013). The leading present-day astronomical parameters include long orbital eccentricity (405 kyr), short orbital eccentricity (128 kyr and 95 kyr), obliquity (41 kyr), and precession (23 kyr and 19 kyr) cycles (Berger et al., 1992; Laskar et al., 2004, 2011). These parameters affect the timing and geographic distribution of insolation thus acting as a long-term paleoclimatic forcing. Geologists read these cycles using paleoclimate proxy records and link the recognized sedimentary oscillations to the astronomical cycles (Hinnov and Hilgen, 2012). However, this involves multiple ongoing scientific challenges: the uncertain nature of linkages between astronomical forcing and paleoclimate proxies (Hinnov, 2013; Weedon, 2003), potentially low signal to noise ratios in paleoclimate proxy series (Kemp, 2016; Meyers, 2012; Mann and Lees, 1996), confirmation of an astronomical origin in

* Corresponding author.
E-mail address: mul450@psu.edu (M. Li).

https://doi.org/10.1016/j.epsl.2018.08.041
0012-821X/

successions of stratigraphic oscillations (Malinverno et al., 2010; Meyers, 2015; Meyers and Sageman, 2007), distortion of the astronomical signal due to variable sedimentation rates (Sinnaesel et al., 2016; Lin et al., 2014; Weedon, 2003; Yu and Ding, 1998), and integration of cyclostratigraphy with other dating tools (Kuiper et al., 2008; Westerhold et al., 2012), among others.

Here we jointly test the astronomical origin of stratigraphic cycles as measured by paleoclimate proxy data, and estimate the evolution of sedimentation rates along a stratigraphic succession. Our approach employs the correlation coefficient between the power spectra of a proxy series and that of an associated astronomical forcing series, converting the proxy series to time for a range of "test" sedimentation rates. The number of astronomical parameters contributing to the estimated sedimentation rates is taken into account. The null hypothesis of no astronomical forcing is tested using a Monte Carlo simulation approach. A sliding window is applied to the proxy series in order to track changes in sedimentation rate along the stratigraphic succession; thus, we call this the "eCOCO" (evolutionary correlation coefficient) method. The eCOCO method is inspired by the average spectral misfit (ASM) method of Meyers and Sageman (2007), the Bayesian Monte Carlo method of Malinverno et al. (2010) and the TimeOpt method of Meyers (2015); similarities and differences among these methods are discussed below.

The eCOCO method is demonstrated using three synthetic series, and three Phanerozoic paleoclimate proxy series. The transition of the late Paleocene through the early Eocene is characterized by a sequence of significant climate events, including the Paleocene–Eocene Thermal Maximum (PETM) and the Eocene Thermal Maximum 2 (ETM2) events. Cyclostratigraphy of ODP Site 1262 (Leg 208) at Walvis Ridge, South Atlantic Ocean has led to the hypothesis of astronomically forced pacing of the PETM and ETM2 events (Lourens et al., 2005), although this hypothesis has been shown to be complicated in follow-on cyclostratigraphic studies by others (Meyers, 2015; Westerhold et al., 2007, 2008). Differing sedimentation rates for the late Paleocene–early Eocene interval have been proposed (Westerhold et al., 2007, 2008) and only an average sedimentation rate for the PETM-ETM2 interval at Site 1262 has been independently tested (Meyers, 2015). An astronomically tuned time scale of the depth-rank series of continental deposits in the Newark Basin, eastern North America, provides the fundamental basis for the age model of the current Late Triassic time scale (Gradstein et al., 2012; Kent et al., 2017). The late Norian–Rhaetian part of the Newark time scale has been recently supported by the global correlation between cycle calibrated magnetic polarity patterns from the Late Triassic Xujiahe Formation and those from the Newark Supergroup (Li et al., 2017). Cyclostratigraphic study of the Givetian–Frasnian magnetic susceptibility series from the La Thure section of Belgium provides a high-resolution astronomical time scale for the Givetian of the Middle Devonian (De Vleeschouwer et al., 2015). The interpretation of astronomical cycles has been further corroborated by Martinez et al. (2016).

In all three of these Phanerozoic cases, eCOCO-derived high-resolution sedimentation rate results provide new insight into the associated paleoclimatic and paleoenvironmental changes. The eCOCO analysis of our three case studies confirms published sedimentation rates at a high degree of confidence (exceeding 99% significance, i.e., rejection of the null hypothesis at levels of $p < 0.01$). Application of eCOCO in cyclostratigraphy thus has the potential more generally to enhance the reproducibility of astrochronological timescales and contribute to establishing more robust geological age models throughout Earth history.

2. Evolutionary correlation coefficient (eCOCO)

2.1. Correlation coefficient

The correlation coefficient used here is the Pearson product-moment correlation coefficient (Mudelsee, 2014), calculated in MATLAB™ (https://www.mathworks.com/help/matlab/ref/corrcoef.html) as

$$\rho(T, D) = \frac{1}{N-1}\sum_{i=1}^{N}\left(\frac{\overline{T_i - \mu_T}}{\sigma_T}\right)\left(\frac{\overline{D_i - \mu_D}}{\sigma_D}\right) \quad (1)$$

where N is a number of observations of the target (T) or data (D) time series, μ_T and σ_T are the mean and standard deviation of the target, and μ_D and σ_D are the mean and standard deviation of the data series. The correlation coefficient measures the linear correlation between the target (T) and data (D) series, where the target series is the power spectrum of the astronomical solution, and the data series is the power spectrum of proxy time series at a given sedimentation rate. The periodogram is a useful metric of agreement because the associated spectral estimates have a narrow resolution bandwidth compared to common procedures such periodogram smoothing or Multi-Taper Method (MTM) spectral estimation (Thomson, 1982). The periodograms of both astronomical target series and data time series are calculated using MATLAB function *periodogram.m* with a zero padded length of 10,000. The red noise background of the data series is modeled using an AR(1) autoregressive fit to the series using MATLAB function *RedConf.m* by Husson (2014) and is employed so as to only retain spectral features that exceed the estimated red noise background; if the spectral amplitude is less than the estimated mean red noise background at a given frequency f, it is set to 0. The range of $\rho$is between -1 and $+1$, where 1 is a perfect positive correlation, 0 is no correlation, and -1 is a perfect negative correlation.

The highest frequency Milankovitch cycle during the past 249 Ma corresponds to the precession index term at 1/(17 kyr) (Laskar et al., 2004), thus we estimate the correlation coefficient of the periodograms of the target and data series over the frequency range 0 to 0.06 cycles/kyr for Cenozoic and Mesozoic series. The highest frequency of the precession index is 1/(16.4 kyr) at 440 Ma according to Berger and Loutre (1994), and so for the Devonian case study (~384 Ma) we estimate the correlation coefficient over the frequency range 0 to 0.07 cycles/kyr.

For paleoclimate series younger than 249 Ma, both data and target series are obtained using periodograms of paleoclimate series and Laskar astronomical solutions, respectively. For paleoclimate series older than 249 Ma, a target series is constructed as the sum of harmonic functions whose frequencies are given by Berger and Loutre (1994) using an original MATLAB script *period2spectrum.m*.

2.2. Significance level

In this step, we adopt as a null hypothesis (H_0) the existence of no astronomical frequencies in the data series and all spectral peaks higher than an AR(1) background occur by chance. Since the periodogram is not Gaussian-distributed (it is Chi-Squared), standard parameteric distributions for the correlation coefficient ρ are not valid. We instead use a non-parametric Monte Carlo approach to produce a null distribution and to test the null hypothesis of no significant astronomical frequencies, as follows:

(1) The number of peaks of the periodogram higher than an AR(1) background for the paleoclimate data series is counted as n, and the sampling frequency (df) of data is

$$df = 1/(N * dt) \quad (2)$$

where N is number of data and dt is sampling rate of data. Here n is counted automatically and doesn't have to be the number of Milankovitch cycles that are present in the measured data.

(2) The modeled data periodogram is constructed with n half sinewaves with randomly distributed frequencies (e.g., half sinewave peaks) and randomly distributed magnitudes (ranges between 0 and 1). Each half sinewave has a width of $2df$.

(3) We use a Monte Carlo simulation to produce a distribution of values of ρ between the modeled random data periodogram and target periodogram at each tested sedimentation rate.

(4) The values of ρ from the Monte Carlo simulations is used to construct a null distribution. The probability for the corresponding correlation coefficient at the sedimentation rate to have arisen due to random chance can be estimated from this null distribution.

(5) The H_0 significance level indicates a specific correlation coefficient value can occur by chance. The H_0 significance level p is considered to be significant if $p < 0.01$, i.e., we would expect a correlation coefficient as large as is estimated to arise from change less than 1% of the time under the null hypothesis.

As an example, the resulting 2000 Monte Carlo surrogate values of ρ between the target periodogram of the La2004 Laskar solution (55–57 Ma) and modeled data periodograms for Synthetic Series #1 (Fig. 1, see section 3.1) yielded values less than the nominal value of 0.7566 (Fig. 2B). This indicates the null hypothesis of no astronomical signal can be rejected at a 0.05% ($p < 0.0005$) significance level at 4 cm/kyr sedimentation rate, i.e., the significance level of the presence of an astronomical signal is 99.95%.

2.3. Number of contributing astronomical parameters

A high, positive ρ and low H_0 significance level may fail to establish the true sedimentation rate. For example, a high positive ρ may occur when only a few astronomical frequencies are used to evaluate the correlation coefficient. To guard against this false positive problem, the total number of contributing astronomical frequencies defined in the target should be evaluated in the correlation coefficient. The number of contributing astronomical frequencies is influenced by two types of influences: Type A arises from the Fourier transform technique that is applied, and Type B derives from the data periodogram at the tested sedimentation rate.

2.3.1. Type A influence

An evenly spaced data series has a stratigraphic sampling interval of Δd; the sampling time interval of the data series time calibrated to a sedimentation rate (sr) is Δt ($\Delta t = \Delta d/sr$). The Nyquist frequency (f_{nyq}) characterizes the maximum resolvable frequency of the periodogram in both stratigraphic and time domains, and the Rayleigh frequency (f_{ray}) characterizes the resolution of the periodogram in both stratigraphic and time domains. The f_{nyq} and f_{ray} of the periodogram in the time domain are defined as:

$$f_{\mathrm{nyq}} = sr/(2 * \Delta d) \tag{3}$$

$$f_{\mathrm{ray}} = sr/(N * \Delta d) \tag{4}$$

where N is the total number of samples for a given data series.

Meyers and Sageman (2007) note that for very high or very low sr, f_{nyq} and f_{ray} of the data periodogram may fall outside the range of the astronomical frequencies. For example, given a very high sr, f_{ray} can be higher than the frequency of the 405-kyr orbital eccentricity cycle and in some cases even of the shorter 100-kyr orbital eccentricity cycles. Thus fewer astronomical frequencies will contribute to the estimated ρ, and may lead to a high ρ at a sedimentation rate that is unreasonably large. For very low sedimentation rates, f_{nyq} may be lower than the frequencies of the ~20 kyr precession index (or even lower), leading to fewer astronomical parameters used in ρ estimation.

2.3.2. Type B influence

The Type B influence depends on characteristics of the data periodogram, that is, the peaks of each astronomical frequency band may be detectable in the same band of the series periodogram. The process for estimating the Type B influence is as follows: (1) The data series is time calibrated with a test sedimentation rate; (2) the data periodogram is estimated, and the data AR(1) spectrum is estimated and "removed" as per the procedure described in section 2.1. If the spectral amplitude in a given astronomical frequency band (Fig. 2 and Supplementary Table 1) is 0 as per our procedure, the corresponding astronomical parameter may not be meaningful. For example, if the spectral amplitude (of age 56 Ma) after accounting for the AR(1) spectrum is zero within the obliquity band of 0.0149–0.0321 cycle/kyr (Supplementary Table 1), this suggests that obliquity forcing was not involved, and the number of contributing astronomical parameters can be reduced by 1.

Variable sedimentation rates lead to widened and/or split peaks in the periodogram (Weedon, 2003), therefore, wide frequency bands of the astronomical target frequencies are adopted in this study. For example, for Synthetic Series #1 (Figs. 1–2, with an age of 55–57 Ma, see below), astronomical target frequency bands are listed in Supplementary Table 1. Because relatively broad frequency bands are used, it is worthwhile to note that the number of specific Milankovitch cycles in the data can be overestimated. And it can be difficult to separate various precession cycles in the paleoclimatic series due to variable sedimentation rates, and sedimentary and climatic processes. However, the result of the number of contributing astronomical parameters is still useful as discussed below.

A result with a low number of contributing astronomical frequencies has two possible interpretations. The first interpretation is that the assigned sedimentation rate is not appropriate. The second interpretation is that one or more astronomical frequencies do not have a significant influence in the data series. The metric that records the number of astronomical frequencies is challenged in geological intervals that are dominated by one astronomical parameter or lack a specific astronomical forcing, such as the Pleistocene obliquity world from 1.2 Ma to 2.7 Ma (Ravelo et al., 2004), or the Early Triassic obliquity dominated intervals in Chinese cyclostratigraphy (Li et al., 2016a). However, even in the well-known Pleistocene obliquity world, 12% of the variance in the δ^{18}O record is in the precession band, whereas 43% is in the obliquity band (Ravelo et al., 2004). Other examples are data series with weak obliquity power from low latitude paleoclimates or hothouses without ice, e.g., the Late Triassic Newark basin (Olsen and Kent, 1996). Therefore, if a low significance level of the null hypothesis derives from the fact that only a few astronomical frequencies were used in the estimation, a high ρ in that case should be considered as suspicious. In other words, the number of Milankovitch cycles that are present in the measured data should be considered if the null hypothesis of no orbital forcing can be rejected.

2.4. Sliding window approach

In our approach, ρ, H_0 significance level and number of contributing astronomical frequencies are made not only for the entire time series, but also along a sliding window along the data series. That is, we begin with a series interval (window) from one end of the series and calculate ρ, H_0 significance level, and the number of contributing astronomical frequencies over a range of sedimentation rates. Then we slide this window for a given step and repeat

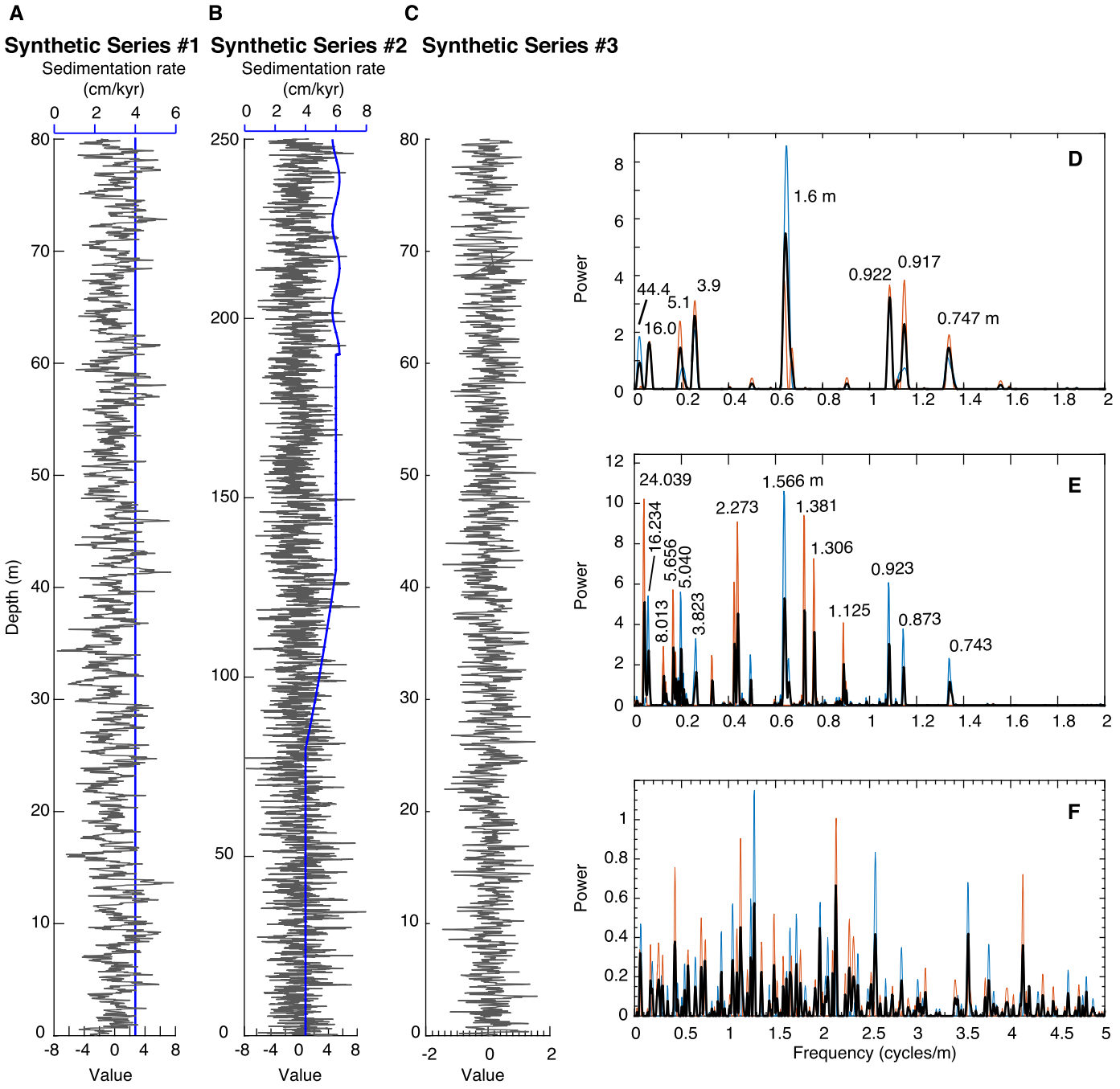

Fig. 1. Three synthetic series and their periodograms. (**A**) Synthetic Series #1 (black) with a 4 cm/kyr sedimentation rate (blue). (**B**) Synthetic Series (#2) with sedimentation rates (blue) from 4 to 6 cm/kyr followed by sine wave oscillations. (**C**) Synthetic Series #3. (**D**) Periodogram of Synthetic Series #1 after removing the AR(1) model. (**E**) Periodogram of Synthetic Series #2 after removing the AR(1) model. (**F**) Periodogram of Synthetic Series #3. (**D**–**F**) Thin blue and thin red lines are periodograms of first and second half slices of the synthetic series. The thick black line is the mean periodogram of the 2 slices. (For interpretation of the colors in the figure(s), the reader is referred to the web version of this article.)

the process until we reach another end of the series. This sliding procedure, termed evolutionary correlation coefficient (eCOCO) analysis detects changing sedimentation rates, as demonstrated in the following synthetic series and three Phanerozoic data series.

3. Forward modeling of the astronomical solutions

3.1. Constant sedimentation rate – Synthetic Series # 1

A 4 cm/kyr sedimentation rate is applied to the Laskar 2004 astronomical solutions of eccentricity, obliquity, and precession index from 55 to 57 Ma (Laskar et al., 2004). This series is added to white noise (normal distribution) and red noise (lag-1 autocorrelation coefficient, $\rho_1 = 0.5$), both with a standard deviation of 1. The original sample rate of the La2004 solution is 1 kyr. We thus get a total of 80 m modeled "climate" series with a 0.04 m sampling rates (Fig. 1A).

To increase the degrees of freedom of the periodogram analysis, the whole series was divided into 2 equally sized slices (termed 2-slice COCO analysis). The mean periodogram of the two slices indicate dominant cycles at 44.4 m, 16.0 m, 5.1 m, 3.9 m, 1.6 m, 0.92 m, and 0.75 m (Fig. 1D). The correlation coefficient between the periodogram of Synthetic Series #1 and that of the target Laskar 2004 solution (55–57 Ma) is estimated for a range of sedimentation rates from 1 to 30 cm/kyr with a step of 0.2 cm/kyr.

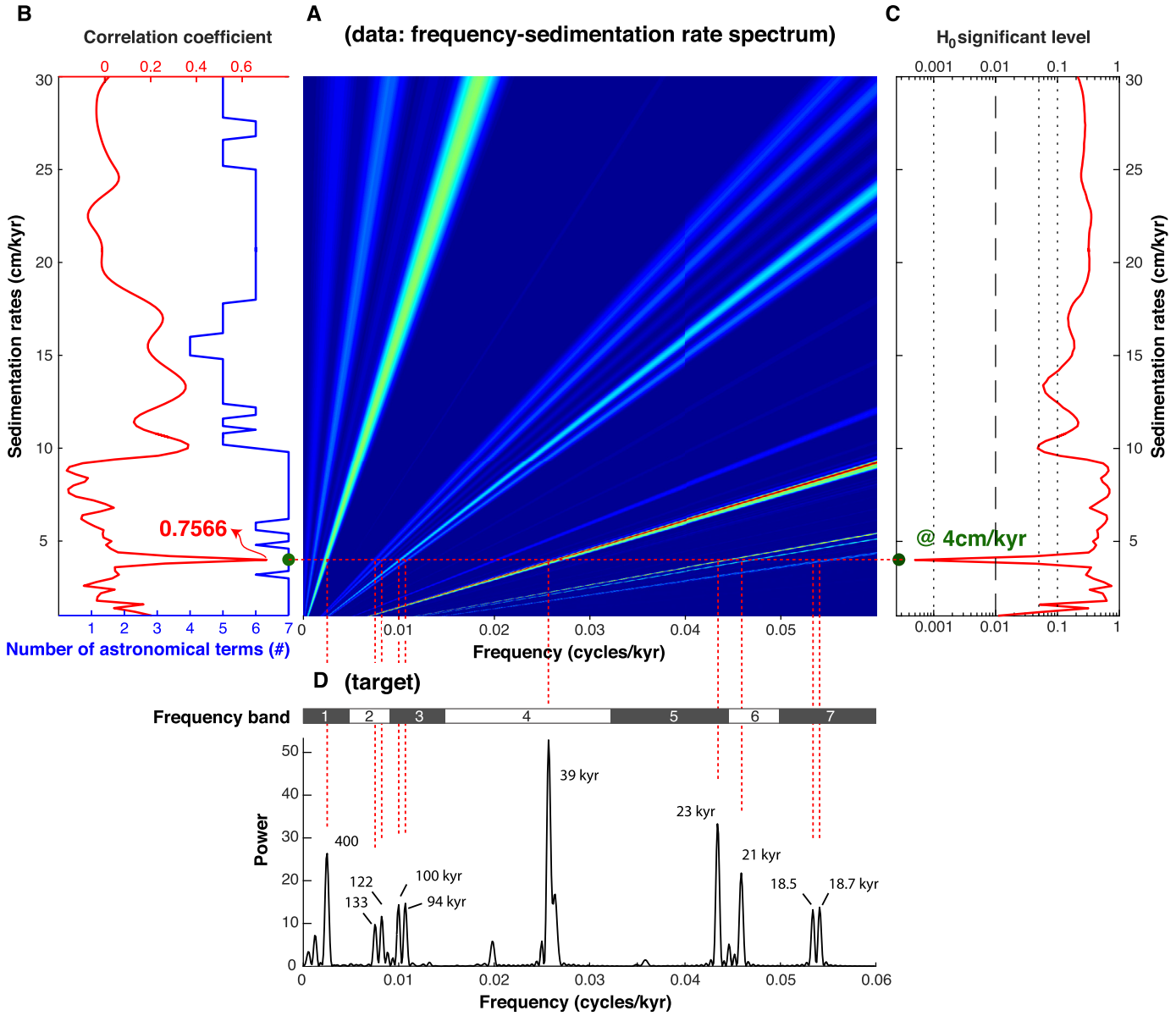

Fig. 2. The eCOCO method. (**A**) Periodograms of Synthetic Series #1 are shown for sedimentation rates ranging from 1 to 30 cm/kyr (vertical axis) and frequencies from 0 to 0.06 cycles/cm (horizontal axis); power is denoted by color (blue = low; red = high). (**B**) The correlation coefficient (black line) and the number of contributing astronomical parameters in the target in the tested sedimentation rate (blue line). (**C**) null hypothesis results. (**D**) Periodogram of the target La2004 astronomical solution (55–57 Ma) (Laskar et al., 2004). The correlation coefficient of the periodograms of Time Series #1 (**A**) and astronomical target periodogram (**D**) indicates a peak at 4 cm/kyr ($\rho = 0.7566$), which is the modeled 4 cm/kyr sedimentation rate. The null hypothesis significance level (H_0-SL) is 0.0005 (0.05%). Seven astronomical parameters are included for the 4 cm/kyr sedimentation rate. Dashed red lines indicate potential locations for astronomical frequencies at a sedimentation rate of 4 cm/kyr. Synthetic Series #1 is calibrated to time over a sedimentation rate range from 1 to 30 cm/kyr and a step of 0.2 cm/kyr. Significance levels are estimated using Monte Carlo simulation with 2000 iterations, which takes 234 s wall clock time.

The evolutionary correlation coefficient curve shows only one peak at 4 cm/kyr where the correlation coefficient reaches a peak at 0.7566, for which the H_0 hypothesis indicates a 0.05% significance level (Fig. 2). The sedimentation rate is 4 cm/kyr and all seven astronomical frequencies in the target (i.e., 405 kyr long orbital eccentricity, 125 kyr and 95 kyr short orbital eccentricity, 39 kyr obliquity, and the 23 kyr, 22 kyr, and 19 kyr precession index) are involved (Fig. 2D). These results strongly support the hypothesis that Synthetic Series #1 has an astronomical signal (significance level at 99.95%).

3.2. *Variable sedimentation rates – Synthetic Series #2*

Variable sedimentation rates, if not accounted and corrected for, result in distortion of periodograms (Weedon, 2003). This hampers the usefulness of the ratio method for cyclostratigraphy. Our sliding window technique obviates this problem.

To demonstrate the ability of eCOCO to identify time-varying sedimentation rates, we use the Laskar 2004 astronomical solution (Laskar et al., 2004) from 53 Ma to 59 Ma to construct a synthetic series. This series is added to a white noise (normal distribution) and a red noise ($\rho_1 = 0.5$) signal, both are with a standard deviation of 1. The modeled sedimentation rate is 4 cm/kyr for the first 2 Myr, then increases from 4 to 6 cm/kyr over the next 1 Myr. The sedimentation rate remains constant at 6 cm/kyr for 1 Myr and then experiences a sine-wave sedimentation rate oscillation for the final 1 Myr (blue line in Fig. 1B). The original sample rate of the La2004 solution is 1 kyr. We thus get a total of 250 m modeled "climate" series with an interpolated 0.04 m sampling rate (black curve in Fig. 1B).

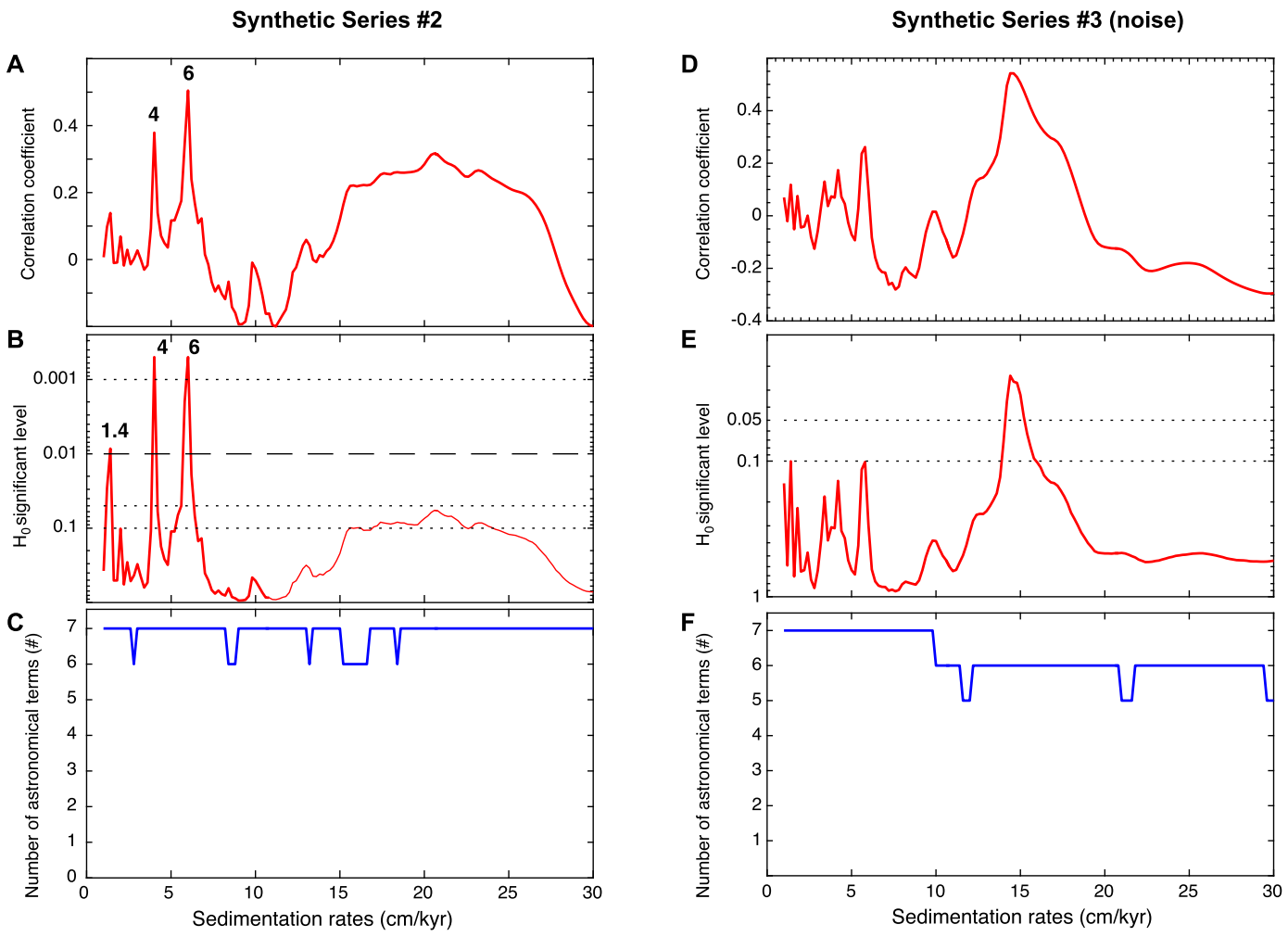

Fig. 3. COCO analysis of Synthetic Series #2 (**A**–**C**) and Synthetic Series #3 (**D**–**F**). (**A** and **D**) The 2-slice COCO analysis shown with labeled potential sedimentation rates. (**B** and **E**) Null hypothesis (H_0, no astronomical forcing) tests indicate that only modeled 4 and 6 cm/kyr sedimentation rates have H_0 significance levels less than 0.001 for Synthetic Series #2 (**B**) and the null hypothesis cannot be rejected at the 1% significance level for the Synthetic Series #3 (**E**). Significance levels are estimated using Monte Carlo simulation of 2000 iterations. (**C** and **F**) The number of contributing astronomical parameters in tested sedimentation rate. Series #2: The astronomical target series is the La2004 astronomical solution from 55 Ma to 57 Ma (Laskar et al., 2004). Synthetic Series #3: The target series is the La2004 astronomical solution from 0–2 Ma. Sedimentation rates range from 1 to 30 cm/kyr with a step of 0.2 cm/kyr.

The two-slice periodogram of Synthetic Series #2 shows multiple peaks at 24.0 m, 16.2 m, 8.0 m, 6.1 m, 5.7 m, 5.0 m, 3.8 m, 2.3 m, 1.6 m, 1.4 m, 1.3 m, 1.1 m, 0.92 m, 0.87 m, and 0.74 m. This makes it hard to apply the astronomical cycle ratio method (Weedon, 2003) (Fig. 1E). In the 2-slice correlation coefficient graphs, three peaks are at 4.0 cm/kyr, 6.0 cm/kyr, and ~20 cm/kyr (Fig. 3A). The H_0 significance levels at the 4 cm/kyr and 6 cm/kyr are lower than 0.1%, and lower than 5.7% at 20.6 cm/kyr. Note that H_0 significance level is as low as 0.85% at 1.4 cm/kyr, however, the correlation coefficient is only 0.1426 (Fig. 3). All 7 astronomical frequencies are used at 4.0 and 6.0 cm/kyr sedimentation rates (Fig. 4E). This strongly suggests that astronomical forcing paced this "climate" series with sedimentation rates at 4.0 and 6.0 cm/kyr.

When we apply the eCOCO method to Synthetic Series #2, the intervals of constant and variable sedimentation rates can clearly be recognized. From a refined survey using a slightly narrowed sedimentation rate grid (from 2 to 10 cm/kyr with a 0.05 cm/kyr step, running window of 25 m) based on the results of the above COCO analysis, eCOCO is displayed as a sedimentation rate map with respect to stratigraphic position. The estimated sedimentation rate is constant from 0 m to 80 m, then increases from 80 to 130 m, stabilizes from 130 to 190 m, and then shows minor oscillations to the end of the series (Fig. 4). These estimated sedimentation rates match well with the original modeled sedimentation rate (blue lines in Fig. 4).

3.3. Red and white noise series – Synthetic Series #3

We apply the COCO method to Synthetic Series #3 (Fig. 1C). Synthetic Series # 3 merges a red noise series ($\rho_1 = 0.5$, standard deviation = 1) and a white noise series (standard deviation = 0.2) simulating random measurement errors, from 0 to 80 m with a sample rate of 0.04 cm. The estimated ρ results display multiple peaks. However, H_0 significance levels of these peaks are never lower than 0.01, suggesting that the null hypothesis cannot be rejected at the 1% level. That, the Synthetic Series # 3 is not influenced by astronomical forcing and no reliable sedimentation rate is available.

4. Application to Phanerozoic paleoclimate series

4.1. Cenozoic: iron series of the PETM-ETM2 interval at ODP Site 1262, Walvis Ridge

ODP Site 1262 from Leg 208 at Walvis Ridge provides a complete record for the Paleogene through the early Eocene from

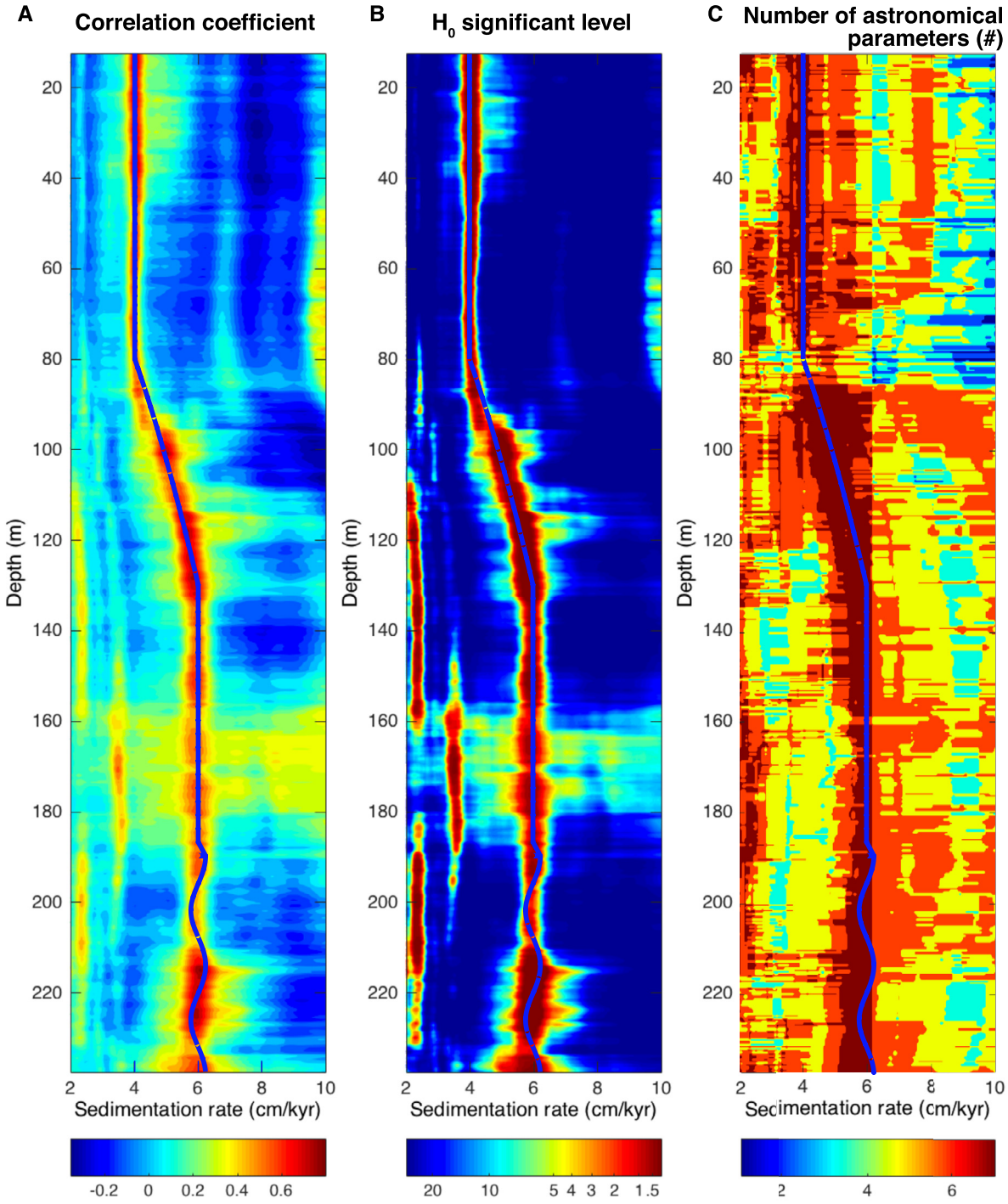

Fig. 4. Refined eCOCO sedimentation rate map of Synthetic Series #2 (Fig. 1B) shown with modeled sedimentation rates (blue lines in Fig. 1B). (**A**) Evolutionary correlation coefficient. (**B**) Evolutionary H_0 significance level. (**C**) Evolutionary map of the number of contributing astronomical parameters. The sliding window size is 25 m; the number of Monte Carlo simulations is 2000. Sedimentation rate from 2 to 10 cm/kyr with a step of 0.05 cm/kyr.

the South Atlantic. Study of this record has enabled an estimation of the duration of the magnetic polarity zones C24r and C25n, and the time of the most prominent Paleogene events, including the Early–Late Paleocene Biotic Event (ELPE), the PETM, and the ETM2. Cyclostratigraphic study by Lourens et al. (2005) on the magnetic susceptibility (MS) and color reflectance (L*, black/white ratio) series at site 1262 indicated that both the PETM and ETM2 events occurred at the maxima in the 405-kyr and 100-kyr cycles that post-date 2.2 myr eccentricity cycle minima, thus, both events were likely astronomically paced. The subsequent cyclostratigraphic research was conducted by Westerhold et al. (2007) on the XRF iron dataset and a* color reflectance (red/green ratio). Westerhold et al. (2007, 2012) further refined the chronology for the magnetostratigraphy and biostratigraphy and proposed that the potential astronomical forcing on the thermal maxima events was complex.

The reported sedimentation rates based on astrochronology, magnetostratigraphy, and biostratigraphy are generally consistent with each other. Paleogene pelagic sediments are characterized by moderate sedimentation rates (~0.6–1.5 cm/kyr), with sedimentation rates up to 1.2 cm/kyr at the PETM interval (Zachos et al., 2004). Assuming each recognized precession cycle lasts 21 kyr, the

resulting sedimentation rates show minor variations throughout the records with a mean value of 1.2 cm/kyr (Westerhold et al., 2007). Meyers (2015) revisited the a* data from Site 1262, focusing on the interval between the PETM and ETM2 spanning 22.4 m. The independent technique "TimeOpt" suggested a mean sedimentation rate of 1.33 cm/kyr for this interval (Meyers, 2015). As shown below, all these estimates are strongly supported by COCO; the eCOCO sedimentation rate map generally matches with the sedimentation rate estimates of Westerhold et al. (2007, 2012).

The Fe series from 111 m to 170 m at Site 1262 was log-transformed and linearly interpolated to a sampling rate of 0.04 m. The series was detrended via removing a 10-m rloess (Cleveland, 1979; robust version of the local regression using weighted linear least squares and a 2nd degree polynomial model) trend. The AR(1) coefficient of the interpolated and detrended Fe series is 0.679. The AR(1) red noise spectrum was removed from the periodogram of the detrended Fe series. We carried out a COCO analysis using the resulting periodogram of the Fe series. Initial COCO analysis suggests a sedimentation rate of 1.4 cm/kyr with a lower than 1% significance level, with power at all 7 astronomical frequency bands (Fig. 6A and Supplementary Table 1). Then a refined COCO analysis with 2000 Monte Carlo simulations was performed on sedimentation rates from 0.5 to 3 cm/kyr. Three peaks at 0.73 cm/kyr, 0.98 cm/kyr and 1.21 cm/kyr emerge in this COCO analysis (Fig. 6B). All of these three sedimentation rates have significance levels lower than 1% and all 7 astronomical frequencies were used in the estimation.

The eCOCO analysis of ρ, H_0 and the number of contributing astronomical frequencies can be used to test the various sedimentation rate estimates of Westerhold et al. (2007, 2008) and mean sedimentation rate for the PETM-ETM 2 interval of Meyers (2015). Abrupt sedimentation rate shifts from 0.75 to 1.3 cm/kyr at 165 m, and from 1.3 to 1.1 cm/kyr at 163.5 m, are consistent with the two options of Westerhold et al. (2007, 2008). However, a slow increase in sedimentation rates from 1.0 to 1.6 cm/kyr at the 159 m to 156.5 m is not (Fig. 7A). The models of Westerhold et al. (2007, 2008) show a drop in the sedimentation rate from 1.6 to 1.2 cm/kyr at 154 m to 153 m. The sedimentation rates in Option 1 by Westerhold et al. (2008) for the 140 m to 155 m interval is supported by eCOCO.

The PETM interval at Site 1262 is characterized by an abruptly decreased sedimentation rate due to the effect of carbonate dissolution (Bralower et al., 2002; Zachos et al., 2005). The eCOCO results indicate a decrease from 1.1 to 0.6 cm/kyr from 141 m to 139 m at Site 1262. Then the sedimentation rate returned to a relatively constant mean sedimentation rate of 1.33 cm/kyr with minor fluctuations from 139 m to 129 m (Fig. 7). No reliable sedimentation rate from eCOCO is detected from 129 m to 122 m; in comparison, Westerhold et al. (2007, 2008) and Meyers (2015) suggest a relatively constant sedimentation rate at 1.3 cm/kyr. Sedimentation rates of 1.3 to 0.7 cm/kyr are indicated by eCOCO for 122 m to the top of the series. This strongly supports the result of the Option #1 presented by Westerhold et al. (2008).

eCOCO sedimentation rates can be applied for depth-to-time transformation of the Fe series. The time-calibrated Fe series indicates that ELMO (ETM-2) occurred ~2.0 Myr after the onset of PETM; this is consistent with the time model of Lourens et al. (2005) but slightly longer than those of Westerhold et al. (2007, 2008) and Meyers (2015). The Fe time series also indicates that both PETM and ELMO occurred during maxima in the 405-kyr and ~100-kyr cycles that post-date very long eccentricity minima (Fig. 8; cf. Lourens et al., 2005), suggesting that, besides volcanism (Gutjahr et al., 2017), astronomical forcing was involved in these events: the extreme seasonal contrast during eccentricity maxima increased ocean temperatures, may have triggered the release of methane hydrates (Lourens et al., 2005).

4.2. Mesozoic: Late Triassic Newark depth-rank series, eastern USA

The continental Newark Basin in eastern North America formed during the breakup of the Pangaea Supercontinent in the Triassic. Over a period of more than 30 Myr, the fluvial and lacustrine Newark Supergroup was deposited in the Newark Basin (Kent et al., 2017). Long-period changes in monsoonal-type rainfall led to variations in water depth in the rifting basins. Consequently, the deposits display pronounced transgressive-regressive cycles as the paleolakes deepened or shallowed. The influence of lake level change on sedimentation rate, which is crucial for understanding the paleoclimate changes and the reconstruction of time scale, remains unclear.

Van Houten (1962) recognized a succession of lithologically distinct cycles in lake facies and estimated that these cycles occurred at 10^4 to 10^5 yr, therefore linked to astronomical cycles. These 'Van Houten cycles' have been coded as a depth-rank series of sedimentary facies (Olsen and Kent, 1996) (Fig. 5B). The depth-rank series (0–2000 m) in the Newark Basin is from composited records of the Rutgers, Somerset, Weston, and Martinsville drill cores. The sample rate of the depth-rank series is 0.85 m, this is sufficient to characterize precession cycles considering the mean sedimentation rate of 14–20 cm/kyr (Olsen and Kent, 1996). Power spectra of the depth rank series in the Newark Basin reveal significant wavelengths that correspond to 405 kyr, 125 kyr and 95 kyr eccentricity cycles, 23 kyr and 19 kyr precession cycles (Li et al., 2017; Olsen and Kent, 1996). These enable the astronomical tuning of the magnetic polarity stratigraphy of the Newark Supergroup, thereby forming the basis of the Newark-APTS for the Late Triassic magnetic polarity pattern (Kent et al., 2017). While some correlations to portions of marine magnetostratigraphy remain uncertain (Kent et al., 2017), the Newark-APTS is the fundamental basis for the Late Triassic time scale (Gradstein et al., 2012).

The COCO applied to the whole series indicates a mean sedimentation rate of 15.2 cm/kyr with $\rho = 0.4334$ (Fig. 6C). The null hypothesis (no astronomical forcing) can be rejected at a significance level of less than 0.05%. Other sedimentation rates with a significance level of less than 1% are 3.6 and 4.6 cm/kyr (Fig. 6C). Only at sedimentation rates within the range of 10–30 cm/kyr are all astronomical target frequencies used for the estimation of ρ and H_0 significance level. The COCO analysis strongly supports the view that the sedimentation rates of the Newark depth-rank series of 0–2000 m are generally slowly varying, and range from 13.6 to 15.6 cm/kyr (Fig. 6C). This result is consistent with the results of Olsen and Kent (1996), Kent et al. (2017), and Li et al. (2017).

We can test these previously estimated sedimentation rates for the Newark depth-rank series. eCOCO analysis of the whole Newark series indicates two possible sedimentation rates at 3–5 cm/kyr and 10–18 cm/kyr that yield ρ above 0.3 (Fig. 9B). A decrease in sedimentation rate from 25 to 10 cm/kyr occurs at 1900 m; the evolutionary H_0 significance level map indicates a similar trend of declining sedimentation rates at 1900 m. Two lines of potential sedimentation rate at 3–5 cm/kyr and 10–18 cm/kyr have H_0 significance levels at less than 1% (Fig. 9C). The evolution of contributing astronomical frequencies indicates that only 3 terms are involved for the 3–5 cm/kyr sedimentation rates. In comparison, more than 6 terms are involved at sedimentation rates of 10–18 cm/kyr (Fig. 9D). Considering all aspects together, sedimentation rates of the Newark depth-rank series most likely varied between 10 and 18 cm/kyr, and was probably 21–27 cm/kyr in the 1900 m to 2000 m interval. The evolutionary ρ is shown with published sedimentation rates by Kent et al. (2017) and Li et al. (2017) (Fig. 9A). Compared with the very coarse sedimentation rate curves of these previous studies, the eCOCO sedimentation rates are generally consistent and have a much higher resolution.

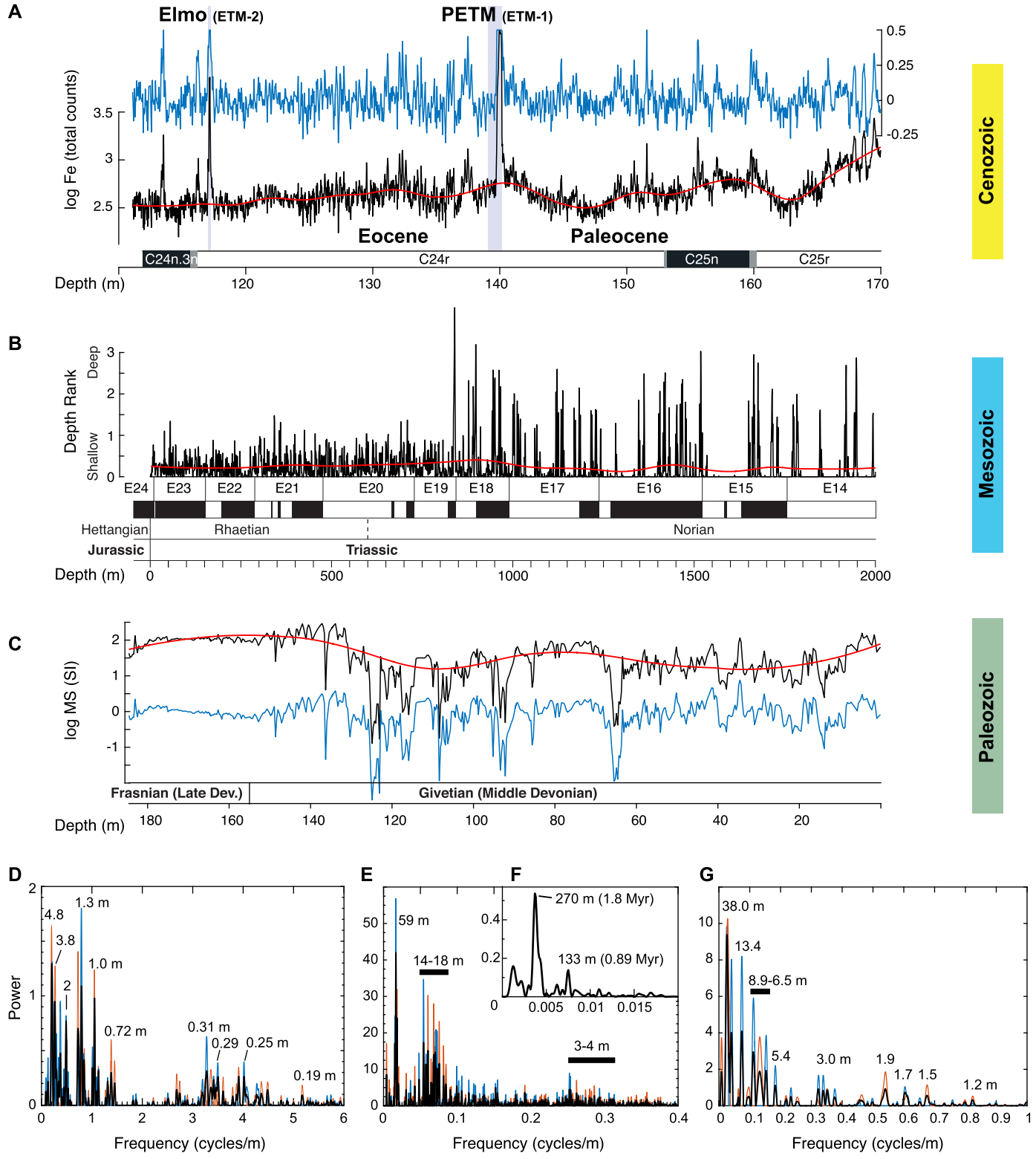

Fig. 5. Phanerozoic paleoclimate series. (**A**) Log-transformed Fe series of ODP site 1262 (black) with a 10-m "rloess" trend (red) and detrended series (blue). Data are from Westerhold et al. (2007, 2008). (**B**) Depth rank series (black) of the Newark Supergroup (Olsen and Kent, 1996) with a 500-m "rloess" trend computed with MATLAB's *smooth*. *m* (red). Magnetic polarity zones are from Kent and Olsen (1999). (**C**) Log-transformed MS series (black) at the La Thure section (De Vleeschouwer et al., 2015) and detrended series (blue) after removing its 80 m "rloess" trend (red). (**D**) 2-slice periodograms of detrended Fe series in (**A**). (**E**) 2-slice periodograms of the detrended depth-rank series in (**B**). (**F**) Periodogram of the Gaussian low-pass filtered depth-rank series (Fig. 8A) after removing third order polynomial trend (cutoff frequency is 0.01 m^{-1}). (**G**) 2-slice periodograms of detrended MS series in (**C**). All detrended series have removed AR(1) models. Thin blue and red lines are periodograms of first and second half slices of the detrended MS series. The thick black line is the mean of periodograms of each slice.

The eCOCO results also reveal recurrent discontinuities in sedimentation rate that coincide with lake level falls with a periodicity of ~270 m. This 270-m recurrence cycle also dominates the low-pass filtered depth-rank series indicative of a long-term lake level cycle (Fig. 5F). Given a mean sedimentation rate of 15.2 cm/kyr (see above), the 270 m cycle represents a 1.78 Myr periodicity,

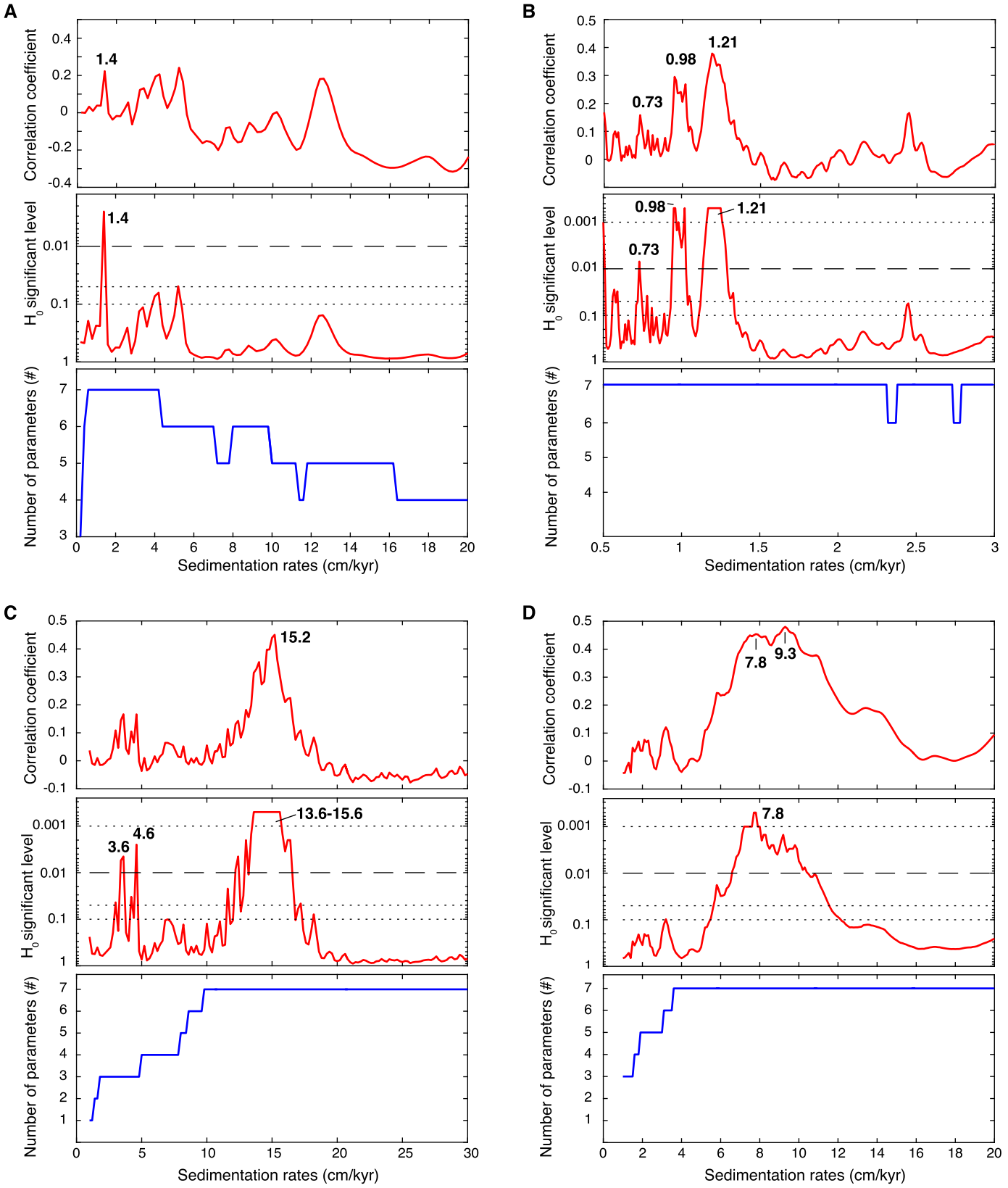

Fig. 6. COCO analysis of the Phanerozoic paleoclimate series. (**A**–**B**) The initial (**A**) and refined (**B**) COCO analysis of the Fe series at ODP Site 1262 and target series (La2004 solution from 55 Ma to 57 Ma). (**A**) is initial test of sedimentation rates ranging from 0.2 to 20 cm/kyr with a step of 0.2 cm/kyr; and (**B**) is refined test focusing on the sedimentation rates from 0.5 to 3 cm/kyr with a step of 0.01 cm/kyr. (**C**) The 2-slice COCO spectra of the Triassic Newark depth-rank series and astronomical target series (La2004 solution from 202 Ma to 204 Ma). Sedimentation rates range from 1 to 30 cm/kyr with a step of 0.2 cm/kyr. (**D**) The 2-slice COCO spectra of the Devonian MS series at the La Thure and target series using Berger94 solution at 384 Ma (Berger and Loutre, 1994). Sedimentation rates range from 1 to 20 cm/kyr with a step of 0.1 cm/kyr. From top to bottom in each panel: the correlation coefficient spectrum; null hypothesis test, and the number of contributing astronomical frequencies. The number of Monte Carlo simulations is 2000.

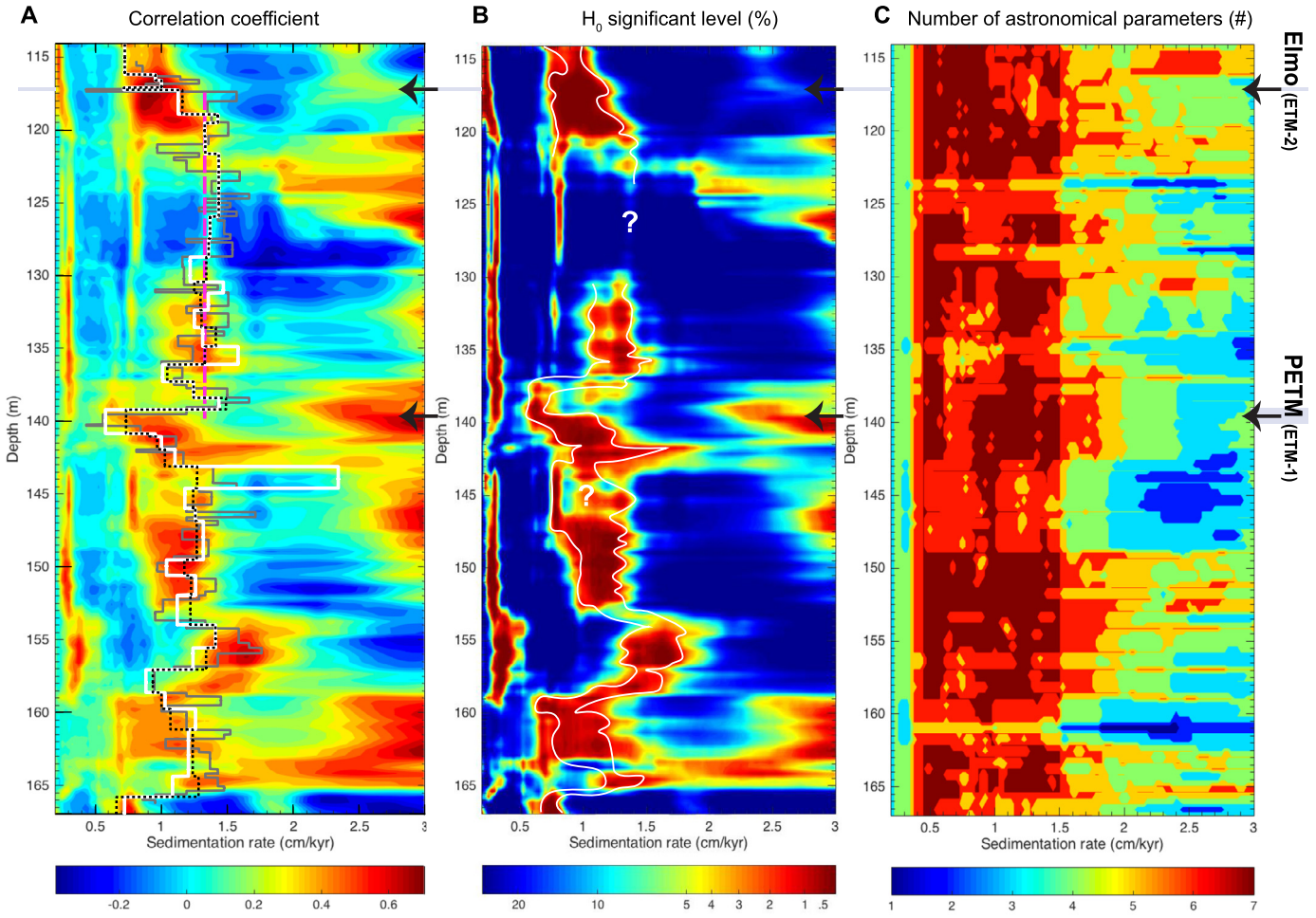

Fig. 7. eCOCO sedimentation rate map of the Fe series at ODP Leg 208 Site 1262. (**A**) Evolutionary ρ shown with published sedimentation rate curves of Westerhold et al. (2007) (grey line) and Westerhold et al. (2008) (dotted black – Option 1; white – Option 2), and Meyers (2015) (dashed pink line). (**B**) Evolutionary H_0 significance level. The area bounded by white lines shows potential sedimentation rates. 122 m to 129 m interval designated with a white "?" has no solution. (**C**) Evolution of the number of contributing astronomical frequencies. The sliding window size is 5 m; the sliding window step is 0.4 m. The number of Monte Carlo simulations is 2000. Sedimentation rates range from 0.2 to 3.0 cm/kyr with a step of 0.01 cm/kyr.

which is comparable to a previously estimated ~1.75 Myr lake level cycle in the Newark Basin (Kent et al., 2017, and references within). The repeated discontinuities in the eCOCO map (Fig. 9B–C) suggest decreased signal-to-noise ratios linked to increased depositional environmental instability and even short-lived erosion during these large lake level falls (cf. Li et al., 2018b). Newark basin lakes experienced a super monsoonal climate due to the Pangaea supercontinent, and the most intense rainy seasons and deepest lakes occurred when precession cycles are configured with perihelion in Northern Hemisphere summer during times of highest eccentricity. The weakest rainy seasons and shallowest lakes occurred when the precession cycle is configured with perihelion during Southern Hemisphere summer during times of lowest eccentricity (Olsen and Kent, 1996). Therefore, eCOCO analysis help understand the driving forcing of sedimentation rate and depositional environmental changes during the Late Triassic.

4.3. Paleozoic: Devonian magnetic susceptibility series from Belgium

Paleozoic cyclostratigraphy is the next frontier in astrochronology (Hinnov, 2013). Here we revisit a 184 m thick Givetian–early Frasnian (~384 Ma, Middle–Late Devonian) magnetic susceptibility (MS) series from the La Thure section, Dinant Synclinorium, southern Belgium (De Vleeschouwer et al., 2015; Martinez et al., 2016). The section is dominated by limestone and shales. The boundary of the Givetian–Frasnian is defined by the first occurrence of conodont *Ancyrodella rotundiloba* and at 155 m ± 2 m at the La Thure section (De Vleeschouwer et al., 2015). The MS series carries a primary depositional signal related to terrestrial input (Pas et al., 2017). De Vleeschouwer et al. (2015) presented a detailed study of the MS series using cyclostratigraphic methods, recognizing a total of 6.5 long orbital eccentricity cycles in the series, suggesting a mean sedimentation rate of 7.0 cm/kyr.

We apply COCO analysis on the MS series. The MS data were log-transformed and interpolated to a 0.3 m sampling rate, and an 80-m 'rloess' trend was removed (Fig. 5C). The periodogram of this series is consistent with those of independent studies by De Vleeschouwer et al. (2015) and Martinez et al. (2016) (Fig. 5F). The La04 and La10 astronomical solutions are restricted to the last 250 Ma; instead the Berger94 solution (Berger and Loutre, 1994) for the new seven astronomical frequencies is used. Linear interpolation at 384 Ma of the Berger94 solution indicates seven astronomical terms: 413, 123, 95 kyr orbital eccentricity cycles, 39.3 and 31.9 kyr obliquity cycles and 19.8 and 16.8 kyr precession index cycles. Two-slice COCO analysis indicates a broad maximum in estimated ρ centered at 8 cm/kyr (Fig. 6D). 2000 Monte Carlo simulations of the null hypothesis test indicates that a wide range of sedimentation rates from 6.6–10.4 cm/kyr exhibits a lower than 1% significance level, and 7.8 cm/kyr lower than 0.1%; thus, the null hypothesis of no astronomical signal can be rejected at a 99.9%

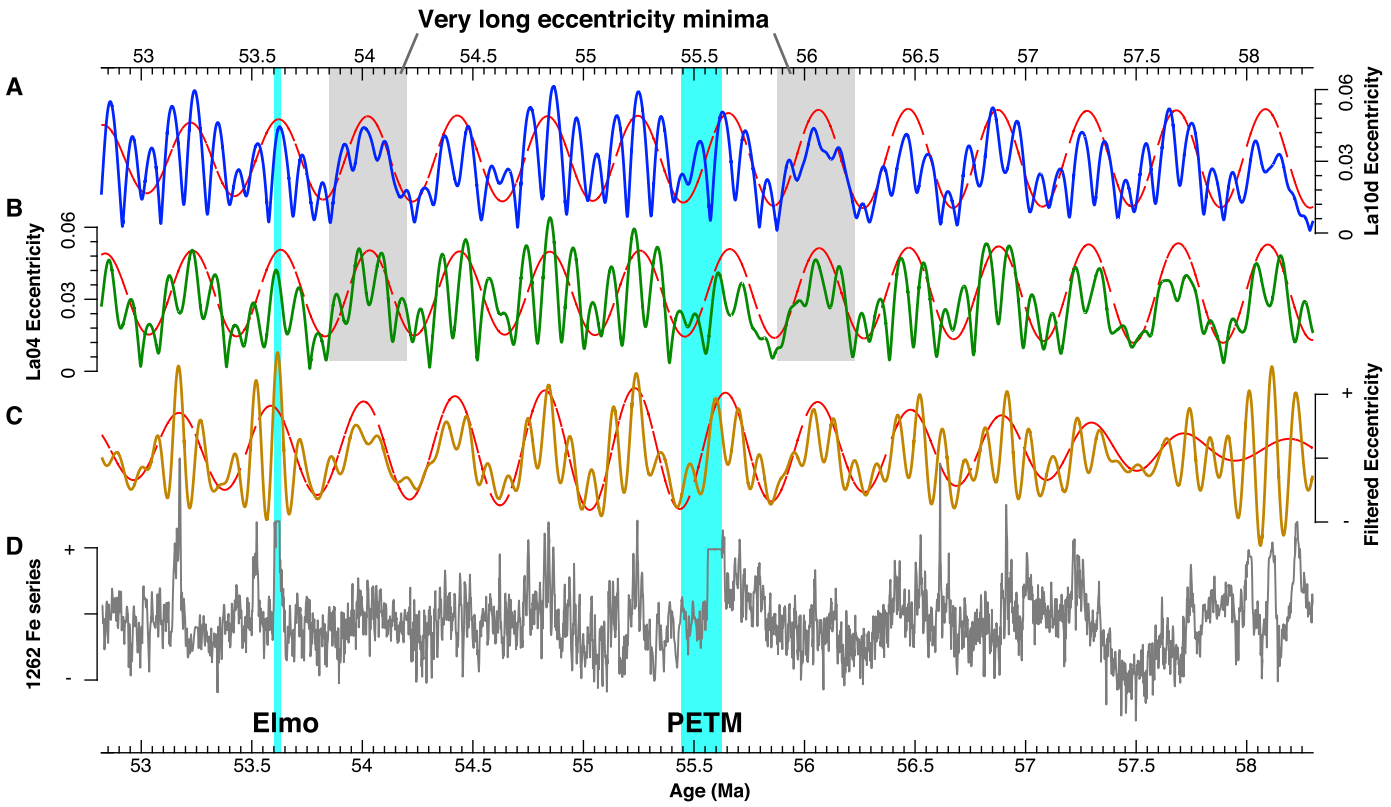

Fig. 8. Time-calibrated ODP Site 1262 Fe series and orbital eccentricity cycles. The Fe series is anchored to La10d solution (Option 1 in Westerhold et al., 2012). Orbital eccentricity solutions of (**A**) La10d (Laskar et al., 2011) and (**B**) La04 (Laskar et al., 2004) with filtered 405-kyr cycles (red dashed, Gaussian filter with a frequency of 0.00248 ± 0.0028 cycles/kyr). (**C**) 405 kyr cycles (red dashed line) and merged 405-kyr and ~100 kyr cycles (orange line, Gaussian filter with a frequency of 0.0098 ± 0.00266 cycles/kyr) of (**D**) the tuned Fe series at Site 1262.

confidence level at 7.8 cm/kyr, with all astronomical frequencies contributing (Fig. 6D).

eCOCO analysis of the La Thure MS series links sedimentation rate to depositional environment (Fig. 10). eCOCO indicates that sedimentation rates range from 6.5 to 10 cm/kyr for 0 m to 65 m, increases up to 13 cm/kyr for 70 m to 100 m, then 6 to 9 cm/kyr for 100 m to 150 m, and slightly increases at the top of the section. The highest sedimentation rate occurs close to the reef of the rimmed shelf, which produces carbonate (Fig. 10A; Pas et al., 2017). The change in sedimentation rate is discontinuous at ~100 m indicating a brief gap and a sea level fall; this is consistent with an abrupt facies shift recognized by Pas et al. (2017). The existence of the brief gap has been hinted: filtered 405 kyr cycles in Fig. 2 of De Vleeschouwer et al. (2015) within 66 m to 92 m contains only three 100 kyr cycles. The eCOCO results indicate that sedimentation rates were paced by 405-kyr orbital eccentricity cycles. Peaks in the filtered 405 kyr cycles indicate "ephemeral" (temporary) and sudden changes in sedimentation rate at ~50 m, 85 m, 140 m, and the top of the MS series.

5. Discussion

Numerous time-calibration techniques for cyclostratigraphy have been proposed in the literature (see e.g. Hinnov, 2013). The provisional time scale approach takes advantage of available radioisotope dating, magnetic polarity patterns, biostratigraphy and chemostratigraphy (Kuiper et al., 2008; Li et al., 2016b, 2018a; Zhang et al., 2015). The second type of time-calibration matches proxy data to the astronomical target series, i.e., dynamic optimization (Yu and Ding, 1998) and dynamic time warping (Lin et al., 2014; Lisiecki and Lisiecki, 2002). In the classical astronomical "minimal tuning" method (Li et al., 2016b; Muller and MacDonald, 2000; Zhang et al., 2015), appropriate Fourier approaches are applied to transfer data from the stratigraphic domain to the time domain by tracking single, dominating frequencies. The sedimentary wavelengths above a certain noise model level are multiplied by a sedimentation rate and matched with predicted astronomical periods via ratios among the frequencies. The best-matched sedimentation rate is selected to construct an astronomical time scale for the stratigraphic series. Tuning of the series to one astronomical frequency can be used to evaluate the success or failure of the tuning to realign other astronomical cycles (Muller and MacDonald, 2000). "Depth-derived" time scales, with additional age constraints, provide a direct test of the astronomical hypothesis (Huybers and Wunsch, 2004).

Without radioisotopic and other time constraints, three recent astronomical testing categories exist; all involve the problem of finding the variation in sedimentation rate that matches sedimentary cycle wavelengths to astronomical periodicities. The first category evaluates the frequency and amplitude modulations that are inherent in the precession index and obliquity cycles (Hinnov, 2000; Zeeden et al., 2015; Boulila et al., 2018). The second category of statistical astronomical testing takes advantage of the bedding hierarchies relationships (ratios of cycles), including the average spectral misfit (ASM) (Meyers and Sageman, 2007) and Bayesian Monte Carlo (Malinverno et al., 2010) approaches. The third category is the inverse approach of time scale optimization that evaluates eccentricity-related amplitude modulation and bundling combining both astronomical amplitude and frequency modulation and bedding hierarchies (Meyers, 2015).

Our technique falls into the second category of statistical astronomical testing that seeks to evaluate frequency ratios as predicted in astronomical solutions. Both ASM and Bayesian Monte Carlo approaches provide statistics on the evaluated sedimentation

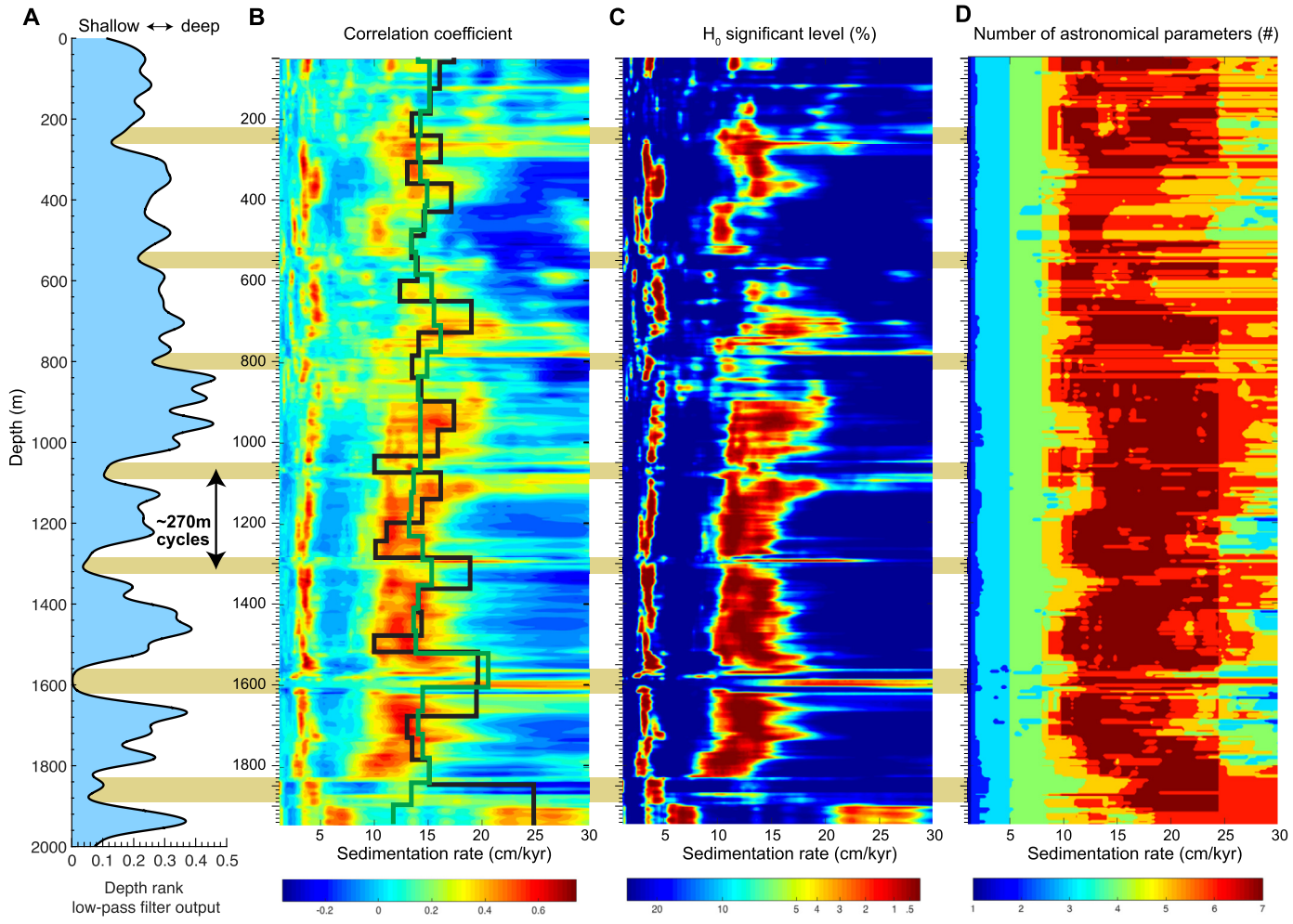

Fig. 9. eCOCO analysis of the Late Triassic Newark depth-rank series (0–2000 m). (**A**). Gaussian low-pass filter output of the depth rank series (cutoff frequency is 0.01 m^{-1}) indicative of latest Triassic lake levels in the Newark Basin shown with ~270 m cycles (gold horizontal bars). (**B**) Evolutionary ρ map shown with published sedimentation rate curves by Kent et al. (2017) (black line) and Li et al. (2017) (green line). (**C**) Evolutionary H_0 significance level map. (**D**) An evolutionary map of the number of contributing astronomical parameters. The sliding window size is 100 m; the step is 5.1 m. All periodograms were analyzed with AR(1) models removed. The number of Monte Carlo simulations is 2000. Sedimentation rates range from 1 to 30 cm/kyr with a step of 0.2 cm/kyr.

rates; the ASM approach also evaluates the null hypothesis of astronomical forcing. Therefore, both ASM and Bayesian Monte Carlo approaches address similar questions with the COCO technique.

These three measurements of fit are not identical. The ASM evaluates the difference between target astronomical frequencies and the frequencies of spectral peaks in the observed data (Meyers and Sageman, 2007); the Bayesian Monte Carlo approach is based on the likelihood of astronomical signals in the periodogram of the measured data (Malinverno et al., 2010); and the COCO method uses the correlation coefficient between the power spectra of a proxy series and an astronomical solution. Generally speaking, the appropriate sedimentation rate leads to low ASM value and lower H_0 significance level in the ASM estimation and higher likelihood in the Bayesian Monte Carlo approach. In comparison, it results in a high correlation coefficient, lower H_0 significance levels, and generally larger number of contributing orbital parameters in the COCO estimation.

Both the ASM and COCO methods yield H_0 significance level, but they are not identical. In the ASM, an indicator of the rejection or acceptance of the null hypothesis is called the critical significance level, which is the inverse of the number of tested sedimentation rates (Meyers and Sageman, 2007). By comparison, our H_0 significance level can be used directly, i.e., the null hypothesis (no orbital forcing) may be rejected if the H_0 significance level in the COCO estimation is lower than 1%, which suggests the confidence level of astronomical forcing is higher than 99%.

6. Conclusions

We have presented a quantitative technique that involves estimating correlation coefficients (COCO) between the periodograms of an astronomical forcing target and paleoclimate series allowing for a variable relationship between time and sedimentation rate. The number of contributing orbital parameters in the estimation of the correlation coefficient is evaluated at each tested sedimentation rate. The hypothesis that astronomical forcing has an impact on the paleoclimate series is tested against a null hypothesis (H_0) of no astronomical forcing. The null distribution is established via a Monte Carlo approach that involves generating surrogate correlation coefficients between the power spectrum of the target and spectra constructed from random frequencies with random spectral amplitudes. The null hypothesis is rejected if the H_0 significance level is lower than 1% ($p < 0.01$) as estimated from the null distribution.

eCOCO analysis performs this procedure with a sliding window to track the variable sedimentation rate, yielding evolutionary (i.e. time-evolving) estimates of the correlation coefficient ρ, H_0 significance level, and the number of contributing astronomical frequencies. eCOCO analysis successfully tracks modeled sedimentation

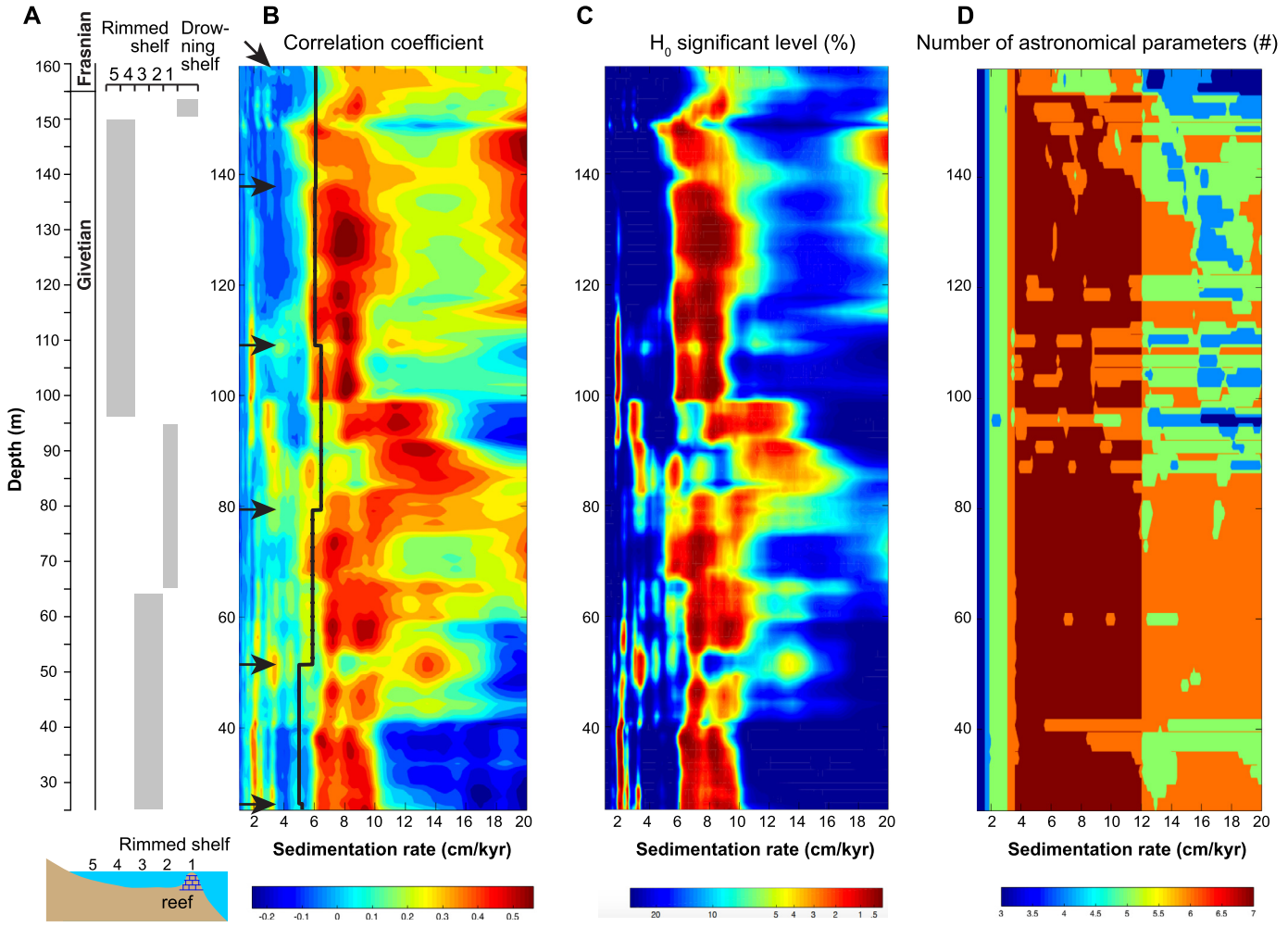

Fig. 10. eCOCO spectra of the log-transformed and detrended La Thure MS series shown with main facies at the La Thure section. (**A**) Main facies of the La Thure section indicative of depositional environments modified from Pas et al. (2017). (**B**) Evolutionary correlation coefficient sedimentation rate map estimated from filtered long-eccentricity peaks in De Vleeschouwer et al. (2015) (see their Fig. 2). Black arrows indicate long-eccentricity peaks in De Vleeschouwer et al. (2015) that interpret changes in sedimentation rates. (**C**) The evolutionary map of the H_0 significance level. (**D**) The evolutionary map of the number of contributing astronomical parameters. The sliding window size is 50 m; the sliding step is 1.2 m. The number of Monte Carlo simulations is 2000. Sedimentation rates range from 1 to 20 cm/kyr with a step of 0.1 cm/kyr.

rates in two synthetic series with constant and variable sedimentation rates. A representative synthetic noise series, by contrast, fails to detect an astronomical signal, with H_0 significance levels at each tested sedimentation rates larger than 1%.

COCO and eCOCO analysis is applied to three Phanerozoic paleoclimate series, including the Paleocene–Eocene Fe series at ODP Leg 208 Site 1262, the Late Triassic depth-rank series in the Newark basin of North America, and the Middle–Late Devonian MS series of the La Thure section, Belgium. The analysis verifies previously established sedimentation rate estimates, while providing new insights into depositional environment changes. In certain instances, our approach reveals previously unidentified changes in sedimentation rate. In summary, COCO and eCOCO analysis is a powerful tool for the evaluation of astronomical forcing of paleoclimate series and sedimentation rate variations. This approach offers new prospects for improving the reproducibility of cyclostratigraphic estimates and improving geological age models throughout the Phanerozoic.

Data availability

The Fe series at ODP Site 1262 is online at https://doi.org/10.1594/PANGAEA.603177 and https://doi.org/10.1594/PANGAEA.667122. The Late Triassic Newark depth-rank series is online at www.ldeo.columbia.edu/~polsen/nbcp/data.html. The Middle–Late Devonian magnetic susceptibility series at the La Thure section is available at https://doi.pangaea.de/10.1594/PANGAEA.855764.

Code availability

The code to generate correlation coefficient and evolutionary correlation coefficient spectra is available in the software *ACycle v 0.1.3*, available at https://github.com/mingsongli/acycle.

Acknowledgements

This research was funded by Heising-Simons Foundation (2016-11). We thank Mathieu Martinez and one anonymous reviewer for their constructive comments. We gratefully acknowledge suggestions from Richard Zeebe. The authors thank Thomas Westerhold, Ursula Röhl, Paul Olsen, David De Vleeschouwer, and Damien Pas for open-sourcing the paleoclimate series. This is a contribution to the IGCP Project 630 and 652.

Appendix A. Supplementary material

Supplementary material related to this article can be found online at https://doi.org/10.1016/j.epsl.2018.08.041.

References

Berger, A., Loutre, M.-F., Laskar, J., 1992. Stability of the astronomical frequencies over the Earth's history for paleoclimate studies. Science 255, 560–566.

Berger, A., Loutre, M.F., 1994. Astronomical forcing through geological time. In: De Boer, P.L., Smith, D.G. (Eds.), Orbital Forcing and Cyclic Sequences. In: IAS Spec. Publ., pp. 15–24.

Boulila, S., et al., 2018. Towards a robust and consistent middle Eocene astronomical timescale. Earth Planet. Sci. Lett. 486, 94–107.

Bralower, T.J., Silva, I.P., Malone, M.J., 2002. New evidence for abrupt climate change in the Cretaceous and Paleogene: an Ocean Drilling Program expedition to Shatsky Rise, northwest Pacific. GSA Today 12, 4–10.

Cleveland, W.S., 1979. Robust locally weighted regression and smoothing scatterplots. J. Am. Stat. Assoc. 74, 829–836.

De Vleeschouwer, D., Boulvain, F., Da Silva, A.-C., Pas, D., Labaye, C., Claeys, P., 2015. The astronomical calibration of the Givetian (Middle Devonian) timescale (Dinant Synclinorium, Belgium). Geol. Soc. (Lond.) Spec. Publ. 414, 245–256.

Gradstein, F., Ogg, J., Schmitz, M., Ogg, G., 2012. The Geological Time Scale 2012. Elsevier, 1144 p.

Gutjahr, M., Ridgwell, A., Sexton, P.F., Anagnostou, E., Pearson, P.N., Pälike, H., Norris, R.D., Thomas, E., Foster, G.L., 2017. Very large release of mostly volcanic carbon during the Palaeocene–Eocene Thermal Maximum. Nature 548, 573–577.

Hinnov, L., 2000. New perspectives on orbitally forced stratigraphy. Annu. Rev. Earth Planet. Sci. 28, 419–475.

Hinnov, L., Hilgen, F.J., 2012. Cyclostratigraphy and astrochronology. In: Gradstein, F., Ogg, J., Schmitz, M., Ogg, G. (Eds.), The Geologic Time Scale 2012. Elsevier, pp. 63–83.

Hinnov, L.A., 2013. Cyclostratigraphy and its revolutionizing applications in the Earth and planetary sciences. Geol. Soc. Am. Bull. 125, 1703–1734.

Husson, D., 2014. MathWorks file exchange: RedNoise_ConfidenceLevels. http://www.mathworks.com/matlabcentral/fileexchange/45539-rednoise-confidencelevels/content/RedNoise_ConfidenceLevels/RedConf.m.

Huybers, P., Wunsch, C., 2004. A depth-derived Pleistocene age model: uncertainty estimates, sedimentation variability, and nonlinear climate change. Paleoceanography 19, PA1028. https://doi.org/10.1029/2002PA000857.

Kemp, D.B., 2016. Optimizing significance testing of astronomical forcing in cyclostratigraphy. Paleoceanography 31, 1516–1531.

Kent, D.V., Olsen, P.E., 1999. Astronomically tuned geomagnetic polarity timescale for the Late Triassic. J. Geophys. Res. 104, 12831–12841.

Kent, D.V., Olsen, P.E., Muttoni, G., 2017. Astrochronostratigraphic Polarity Time Scale (APTS) for the Late Triassic and Early Jurassic from continental sediments and correlation with standard marine stages. Earth-Sci. Rev. 166, 153–180.

Kuiper, K.F., Deino, A., Hilgen, F.J., Krijgsman, W., Renne, P.R., Wijbrans, J.R., 2008. Synchronizing rock clocks of Earth history. Science 320, 500–504.

Laskar, J., Fienga, A., Gastineau, M., Manche, H., 2011. La2010: a new orbital solution for the long-term motion of the Earth. Astron. Astrophys. 532, A89. https://doi.org/10.1051/0004-6361/201116836.

Laskar, J., Robutel, P., Joutel, F., Gastineau, M., Correia, A.C.M., Levrard, B., 2004. A long-term numerical solution for the insolation quantities of the Earth. Astron. Astrophys. 428, 261–285.

Li, M., Huang, C., Hinnov, L., Chen, W., Ogg, J., Tian, W., 2018a. Astrochronology of the Anisian stage (Middle Triassic) at the Guandao reference section, South China. Earth Planet. Sci. Lett. 482, 591–606.

Li, M., Huang, C., Hinnov, L., Ogg, J., Chen, Z.-Q., Zhang, Y., 2016a. Obliquity-forced climate during the Early Triassic hothouse in China. Geology 44, 623–626.

Li, M., Hinnov, L.A., Huang, C., Ogg, J.G., 2018b. Sedimentary noise and sea levels linked to land–ocean water exchange and obliquity forcing. Nat. Commun. 9, 1004. https://doi.org/10.1038/s41467-018-03454-y.

Li, M., Ogg, J., Zhang, Y., Huang, C., Hinnov, L., Chen, Z.-Q., Zou, Z., 2016b. Astronomical-cycle scaling of the end-Permian extinction and the Early Triassic Epoch of South China and Germany. Earth Planet. Sci. Lett. 441, 10–25.

Li, M., Zhang, Y., Huang, C., Ogg, J., Hinnov, L., Wang, Y., Zou, Z., Li, L., 2017. Astronomical tuning and magnetostratigraphy of the Upper Triassic Xujiahe Formation of South China and Newark Supergroup of North America: implications for the Late Triassic time scale. Earth Planet. Sci. Lett. 475, 207–223.

Lin, L., Khider, D., Lisiecki, L.E., Lawrence, C.E., 2014. Probabilistic sequence alignment of stratigraphic records. Paleoceanography 29, 976–989.

Lisiecki, L.E., Lisiecki, P.A., 2002. Application of dynamic programming to the correlation of paleoclimate records. Paleoceanography 17, 1–12.

Lourens, L.J., Sluijs, A., Kroon, D., Zachos, J.C., Thomas, E., Rohl, U., Bowles, J., Raffi, I., 2005. Astronomical pacing of late Palaeocene to early Eocene global warming events. Nature 435, 1083–1087.

Malinverno, A., Erba, E., Herbert, T.D., 2010. Orbital tuning as an inverse problem: chronology of the early Aptian oceanic anoxic event 1a (Selli Level) in the Cismon APTICORE. Paleoceanography 25, PA2203. https://doi.org/10.1029/2009PA001769.

Mann, M.E., Lees, J.M., 1996. Robust estimation of background noise and signal detection in climatic time series. Clim. Change 33, 409–445.

Martinez, M., Kotov, S., De Vleeschouwer, D., Pas, D., Pälike, H., 2016. Testing the impact of stratigraphic uncertainty on spectral analyses of sedimentary series. Clim. Past 12, 1765–1783.

Meyers, S.R., 2015. The evaluation of eccentricity-related amplitude modulation and bundling in paleoclimate data: an inverse approach for astrochronologic testing and time scale optimization. Paleoceanography 30. https://doi.org/10.1002/2015PA002850.

Meyers, S.R., 2012. Seeing red in cyclic stratigraphy: spectral noise estimation for astrochronology. Paleoceanography 27, PA3228. https://doi.org/10.1029/2012PA002307.

Meyers, S.R., Sageman, B.B., 2007. Quantification of deep-time orbital forcing by average spectral misfit. Am. J. Sci. 307, 773–792.

Mudelsee, M., 2014. Climate Time Series Analysis—Classical Statistical and Bootstrap Methods. Springer Verlag, Cham, 454 p.

Muller, R.A., MacDonald, G.J., 2000. Ice Ages and Astronomical Causes: Data, Spectral Analysis, and Mechanisms. Springer-Praxis, London, 318 p.

Olsen, P.E., Kent, D.V., 1996. Milankovitch climate forcing in the tropics of Pangaea during the Late Triassic. Palaeogeogr. Palaeoclimatol. Palaeoecol. 122, 1–26.

Pas, D., Da Silva, A.-C., Devleeschouwer, X., De Vleeschouwer, D., Cornet, P., Labaye, C., Boulvain, F., 2017. Insights into a million-year-scale Rhenohercynian carbonate platform evolution through a multi-disciplinary approach: example of a Givetian carbonate record from Belgium. Geol. Mag. 154, 707–739.

Ravelo, A.C., Andreasen, D.H., Lyle, M., Olivarez Lyle, A., Wara, M.W., 2004. Regional climate shifts caused by gradual global cooling in the Pliocene epoch. Nature 429, 263–267.

Sinnaesel, M., et al., 2016. Astronomical component estimation (ACE v.1) by time-variant sinusoidal modeling. Geosci. Model Dev. 9, 3517–3531.

Thomson, D.J., 1982. Spectrum estimation and harmonic analysis. Proc. IEEE 70, 1055–1096.

Van Houten, F.B., 1962. Cyclic sedimentation and the origin of analcime-rich Upper Triassic Lockatong Formation, west-central New Jersey and adjacent Pennsylvania. Am. J. Sci. 260, 561–576.

Weedon, G.P., 2003. Time Series Analysis and Cyclostratigraphy: Examining Stratigraphic Records of Environmental Cycles. Cambridge University Press.

Westerhold, T., Röhl, U., Laskar, J., 2012. Time scale controversy: accurate orbital calibration of the early Paleogene. Geochem. Geophys. Geosyst. 13, Q06015. https://doi.org/10.1029/2012GC004096.

Westerhold, T., Röhl, U., Laskar, J., Raffi, I., Bowles, J., Lourens, L.J., Zachos, J.C., 2007. On the duration of magnetochrons C24r and C25n and the timing of early Eocene global warming events: implications from the Ocean Drilling Program Leg 208 Walvis Ridge depth transect. Paleoceanography 22, PA2201. https://doi.org/10.1029/2006PA001322.

Westerhold, T., Röhl, U., Raffi, I., Fornaciari, E., Monechi, S., Reale, V., Bowles, J., Evans, H.F., 2008. Astronomical calibration of the Paleocene time. Palaeogeogr. Palaeoclimatol. Palaeoecol. 257, 377–403.

Yu, Z.W., Ding, Z.L., 1998. An automatic orbital tuning method for paleoclimate records. Geophys. Res. Lett. 25, 4525–4528.

Zachos, J.C., Kroon, D., Blum, P., et al., 2004. Proc. ODP, Init. Repts. 208. College Station, TX (Ocean Drilling Program). https://doi.org/10.2973/odp.proc.ir.208.2004.

Zachos, J.C., Röhl, U., Schellenberg, S.A., Sluijs, A., Hodell, D.A., Kelly, D.C., Thomas, E., Nicolo, M., Raffi, I., Lourens, L.J., 2005. Rapid acidification of the ocean during the Paleocene–Eocene thermal maximum. Science 308, 1611–1615.

Zeeden, C., Meyers, S.R., Lourens, L.J., Hilgen, F.J., 2015. Testing astronomically tuned age models. Paleoceanography 30, 369–383. https://doi.org/10.1002/2014PA002762.

Zhang, Y., Li, M., Ogg, J.G., Montgomery, P., Huang, C., Chen, Z.-Q., Shi, Z., Enos, P., Lehrmann, D.J., 2015. Cycle-calibrated magnetostratigraphy of middle Carnian from South China: implications for Late Triassic time scale and termination of the Yangtze Platform. Palaeogeogr. Palaeoclimatol. Palaeoecol. 436, 135–166.